PERGAMON

International Journal of Solids and Structures 37 (2000) 4275–4288

INTERNATIONAL JOURNAL OF SOLIDS and STRUCTURES

www.elsevier.com/locate/ijsolstr

Shell analysis of an inflatable arch subjected to snow and wind loading

Raymond H. Plaut[a,*], Julian K.S. Goh[a], Martin Kigudde[a], Daniel C. Hammerand[b]

[a]*Charles E. Via, Jr., Department of Civil and Environmental Engineering, Virginia Polytechnic Institute and State University, Blacksburg, VA 24061-0105, USA*

[b]*Department of Aerospace and Ocean Engineering, Virginia Polytechnic Institute and State University, Blacksburg, VA 24061-0203, USA*

Received 21 January 1999; in revised form 9 June 1999

Abstract

A flexible material, such as a woven or braided fabric, may be tailored to form an arch when inflated. Such arches have been used as the framework for transportable shelters and are analyzed in this paper. It is assumed that the cross section of the pressurized arch is circular and that only in-plane (membrane) stresses are present. An analytical solution for these initial stresses is given for an arbitrary arch centerline shape. Then external loads are applied, and the additional stress resultants include bending and twisting moments. The linear thin-shell theory of Sanders is used to formulate the governing equations, including the effect of the initial membrane stresses. The material is linearly elastic, nonhomogeneous, and orthotropic. Approximate solutions are obtained using the Rayleigh–Ritz method. In the examples, the centerline of the arch is a semi-circle, the ends are fixed, and the material is homogeneous and isotropic. Four loads are treated: a symmetric ('full') snow load, an asymmmetric ('half') snow load, a wind load symmetric with respect to the plane of the arch centerline, and a distributed load acting sideways. The resulting deflections are computed and plotted.

Keywords: Arches; Elastic; Energy methods; Rayleigh–Ritz method; Sanders theory; Shell; Snow load; Wind load

1. Introduction

A pressurized arch made of a highly flexible material (e.g., a fabric) is analyzed. Such arches have

* Corresponding author. Tel.: +1-540-231-6072; fax: +1-540-231-7532.
E-mail address: rplaut@vt.edu (R.H. Plaut).

0020-7683/00/$ - see front matter
PII: S0020-7683(99)00189-4

been used to support tent-like structures. Some examples of these structures are depicted by Reffell (1967), Price et al. (1971), Dent (1972), Otto (1973), Kronenburg (1995), Kronenburg (1996), Hampel et al. (1996), Galas and Bacskai (1998). They could act as deployable shelters for vehicles, helicopters, and aircraft, and also may have potential use as emergency shelters during or following natural disasters. They can be transported in modules and the arches can be inflated at the site.

The behavior of a single pressurized arch has been considered in several studies. Kawaguchi et al. (1972) described experiments using loads that simulated wind pressure. Steeves (1978) tested a toroidal tube under concentrated and uniform loading conditions, and analyzed such structures assuming linearly elastic behavior, a circular cross section which does not deform, and a membrane state of stress. Collapse of an inflated toroidal membrane subjected to a concentrated load was investigated by Lukasiewicz and Balas (1990).

The finite element method using shell elements has been applied in some recent studies of these structures. Molloy (1998) considered a pressurized arch with a parabolic shape. Snow loads and a wind load were applied, and deflections, vibration frequencies, and buckling loads were determined. Mohan and Kapania (1998a, 1998b) analyzed a circular arch and included large loads and deflections. Their first paper treated a concentrated load at the crown of the arch, whereas the behavior under two external pressure distributions was investigated in their second paper. Kim et al. (1998) examined the response of a shelter supported by ten pressurized arches and subjected to symmetric and asymmetric snow loads. Displacements and vibration frequencies were computed. Finally, Molloy et al. (1999) considered a pair of pressurized arches leaning against each other and attached at the point of contact near their crowns. In conjunction with these numerical studies, experimental tests were carried out on scale models of a shelter supported by flexible arches (Carradine and Plaut, 1998).

In the following section, the arch is considered in its pressurized state prior to the application of service loads. In this state, the arch is assumed to have a circular cross section, and the locus of the centers of the cross sections (the centerline) is assumed to be known (and is not necessarily circular). The associated 'initial stresses' due to the internal pressure are assumed to comprise a membrane state. The equilibrium equations have an analytical solution for the in-plane stress resultants.

In Section 3, the service loads (e.g., snow or wind) are applied to the pressurized arch. The resulting displacements are assumed to be small and a linear analysis is carried out. Both membrane and bending stresses are included, and Sanders' linear thin-shell theory is utilized to formulate the governing equations. The material is assumed to be linearly elastic, and may be nonhomogeneous and orthotropic.

The solution procedure is described in Section 4. It involves the Rayleigh–Ritz method, based on stationarity of the total potential with respect to kinematically admissible variations in the displacements. Numerical results are obtained in Section 5 for symmetric and asymmetric snow loads, a wind load, and a sideways load. Concluding remarks are presented in Section 6.

2. Pressurized state

A side view of the inflated arch is shown in Fig. 1(a). The arc length along the centerline (i.e., the meridional coordinate) is s, with $s = 0$ at the crown, $s = -s_0$ at the left base, and $s = s_0$ at the right base. Fig. 1(b) depicts the cross section, with constant radius r and with circumferential coordinate ϕ (where $\phi = 0$ at the top meridian). The orthogonal curvilinear coordinates s and ϕ are principal coordinates.

The shape of the centerline is denoted by $y(x)$, and the curvature κ is given by

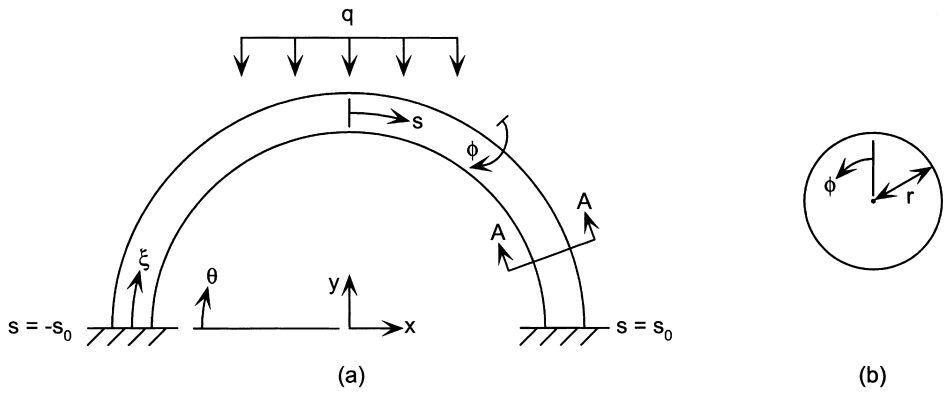

Fig. 1. Geometry of arch: (a) side view; (b) section A–A.

$$\kappa = \frac{-y''}{\left[1+(y')^2\right]^{3/2}} \tag{1}$$

The Lamé parameters A_ϕ and A_s and the principal radii of curvature R_ϕ and R_s are as follows (Kraus, 1967):

$$A_\phi = r, \quad A_s = 1 + r\kappa\cos\phi, \quad R_\phi = r, \quad R_s = r + \frac{1}{\kappa\cos\phi} \tag{2}$$

Fig. 2(a) shows the in-plane stress resultants T_ϕ, T_s, and $T_{\phi s}$ associated with the constant internal pressure p. The equilibrium equations in general form are

$$\frac{\partial}{\partial\phi}\left(A_s T_\phi\right) + \frac{\partial}{\partial s}\left(A_\phi T_{\phi s}\right) + \frac{\partial A_\phi}{\partial s}T_{\phi s} - \frac{\partial A_s}{\partial\phi}T_s = 0 \tag{3a}$$

$$\frac{\partial}{\partial s}\left(A_\phi T_s\right) + \frac{\partial}{\partial\phi}\left(A_s T_{\phi s}\right) + \frac{\partial A_s}{\partial\phi}T_{\phi s} - \frac{\partial A_\phi}{\partial s}T_\phi = 0 \tag{3b}$$

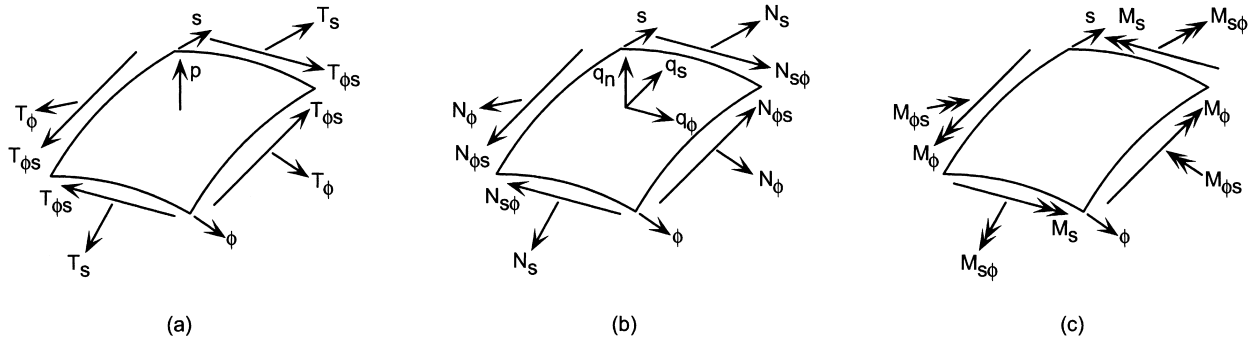

Fig. 2. Stress resultants and loads: (a) initial in-plane stress resultants and internal pressure; (b) additional in-plane stress resultants and service loads; (c) additional moments.

$$\frac{T_\phi}{R_\phi} + \frac{T_s}{R_s} = p \tag{3c}$$

For the case considered in this paper, with constant cross-sectional radius and with Eq. (2) being satisfied, the solution of Eqs. (3a–c) is given by

$$T_\phi(s, \phi) = \frac{pr\left[2 + r\kappa(s)\cos\phi\right]}{2\left[1 + r\kappa(s)\cos\phi\right]}, \quad T_s = \frac{pr}{2}, \quad T_{\phi s} = 0 \tag{4}$$

This analytical solution is well-known for the special case of toroidal shells with circular cross sections, i.e., when κ is constant (e.g., Zingoni, 1997). As seen here, it is also valid when κ is a function of the meridional coordinate s.

3. Service loads

Distributed loads (e.g., snow or wind loads) are applied to the pressurized arch, and the displacements and additional stresses are to be determined. The arch material is assumed to be linearly elastic, nonhomogeneous (or homogeneous), and orthotropic (or isotropic). A linear analysis is assumed to be sufficient, i.e., the displacements under the service loads are assumed to be small. The arch is treated as a thin shell and Sanders' theory (sometimes called Sanders–Koiter theory) is used (Sanders, 1959; Koiter, 1960; Budiansky and Radkowski, 1963; Budiansky and Sanders, 1963; Kraus, 1967; Zhang and Redekop, 1992; Zingoni, 1997).

3.1. Equilibrium

The additional in-plane stress resultants are shown in Fig. 2(b) and the bending and twisting moment resultants (i.e., moments per unit length) are drawn in Fig. 2(c). The transverse shear resultants are not depicted. The surface traction forces per unit area are q_ϕ, q_s, and q_n in the ϕ, s, and normal directions, respectively, with q_n positive if pointing outward, as illustrated in Fig. 2(b).

The modified membrane shear resultant and modified twisting moment resultant are defined as

$$\bar{N}_{\phi s} = \frac{1}{2}\left(N_{\phi s} + N_{s\phi}\right), \qquad \bar{M}_{\phi s} = \frac{1}{2}\left(M_{\phi s} + M_{s\phi}\right) \tag{5}$$

respectively. After elimination of the transverse shear resultants, the resulting equilibrium equations (including the initial stress resultants T_ϕ, T_s, and $T_{\phi s}$) are as follows:

$$\frac{\partial}{\partial\phi}\left(A_s N_\phi\right) + \frac{\partial}{\partial s}\left(A_\phi \bar{N}_{\phi s}\right) + \frac{\partial A_\phi}{\partial s}\bar{N}_{\phi s} - \frac{\partial A_s}{\partial\phi}N_s + \frac{1}{R_\phi}\frac{\partial}{\partial\phi}\left(A_s M_\phi\right)$$

$$+\frac{1}{R_\phi}\frac{\partial}{\partial s}\left(A_\phi \bar{M}_{\phi s}\right) + \frac{1}{R_\phi}\frac{\partial A_\phi}{\partial s}\bar{M}_{\phi s} - \frac{1}{R_\phi}\frac{\partial A_s}{\partial\phi}M_s$$

$$+\frac{1}{2}A_\phi\frac{\partial}{\partial s}\left[\left(\frac{1}{R_\phi} - \frac{1}{R_s}\right)\bar{M}_{\phi s}\right] - \frac{A_\phi A_s}{R_\phi}\left(\beta_\phi T_\phi + \beta_s T_{\phi s}\right) = -A_\phi A_s q_\phi \tag{6a}$$

$$\frac{\partial}{\partial s}\left(A_\phi N_s\right)+\frac{\partial}{\partial \phi}\left(A_s \bar{N}_{\phi s}\right)+\frac{\partial A_s}{\partial \phi}\bar{N}_{\phi s}-\frac{\partial A_\phi}{\partial s}N_\phi+\frac{1}{R_s}\frac{\partial}{\partial s}\left(A_\phi M_s\right)$$

$$+\frac{1}{R_s}\frac{\partial}{\partial \phi}\left(A_s \bar{M}_{\phi s}\right)+\frac{1}{R_s}\frac{\partial A_s}{\partial \phi}\bar{M}_{\phi s}-\frac{1}{R_s}\frac{\partial A_\phi}{\partial s}M_\phi$$

$$+\frac{1}{2}A_s\frac{\partial}{\partial \phi}\left[\left(\frac{1}{R_s}-\frac{1}{R_\phi}\right)\bar{M}_{\phi s}\right]-\frac{A_\phi A_s}{R_s}\left(\beta_s T_s+\beta_\phi T_{\phi s}\right)=-A_\phi A_s q_s \tag{6b}$$

$$\frac{\partial}{\partial \phi}\left\{\frac{1}{A_\phi}\left[\frac{\partial}{\partial \phi}\left(A_s M_\phi\right)+\frac{\partial}{\partial s}\left(A_\phi \bar{M}_{\phi s}\right)+\frac{\partial A_\phi}{\partial s}\bar{M}_{\phi s}-\frac{\partial A_s}{\partial \phi}M_s\right]\right\}$$

$$+\frac{\partial}{\partial s}\left\{\frac{1}{A_s}\left[\frac{\partial}{\partial s}\left(A_\phi M_s\right)+\frac{\partial}{\partial \phi}\left(A_s \bar{M}_{\phi s}\right)+\frac{\partial A_s}{\partial \phi}\bar{M}_{\phi s}-\frac{\partial A_\phi}{\partial s}M_\phi\right]\right\}$$

$$-\left(\frac{N_\phi}{R_\phi}+\frac{N_s}{R_s}\right)A_\phi A_s-\frac{\partial}{\partial \phi}\left[A_s\left(\beta_\phi T_\phi+\beta_s T_{\phi s}\right)\right]-\frac{\partial}{\partial s}\left[A_\phi\left(\beta_s T_s+\beta_\phi T_{\phi s}\right)\right]=-A_\phi A_s q_n \tag{6c}$$

In Eqs. (6a–c), β_ϕ and β_s are rotations and will be defined in Eq. (8).

3.2. Strain–displacement relationships

In the ϕ and s directions, respectively, the extensional strains are ε_ϕ and ε_s, and the bending strains (i.e., changes in curvature) are κ_ϕ and κ_s. The in-plane shearing strain is $\gamma_{\phi s}$ and the twisting strains are $\kappa_{\phi s}$ and $\kappa_{s\phi}$. The modified twisting strain is defined as

$$\bar{\kappa}_{\phi s}=\frac{1}{2}(\kappa_{\phi s}+\kappa_{s\phi}) \tag{7}$$

The mid-surface displacements in the ϕ, s, and normal directions, respectively, are denoted by u_ϕ, u_s, and w, with w positive if outward. Then the rotations β_ϕ and β_s are defined as

$$\beta_\phi=\frac{u_\phi}{R_\phi}-\frac{1}{A_\phi}\frac{\partial w}{\partial \phi},\qquad \beta_s=\frac{u_s}{R_s}-\frac{1}{A_s}\frac{\partial w}{\partial s} \tag{8}$$

The strain–displacement relationships are as follows:

$$\varepsilon_\phi=\frac{1}{A_\phi}\frac{\partial u_\phi}{\partial \phi}+\frac{1}{A_\phi A_s}\frac{\partial A_\phi}{\partial s}u_s+\frac{w}{R_\phi},$$

$$\varepsilon_s=\frac{1}{A_s}\frac{\partial u_s}{\partial s}+\frac{1}{A_\phi A_s}\frac{\partial A_s}{\partial \phi}u_\phi+\frac{w}{R_s},$$

$$\gamma_{\phi s}=\frac{1}{A_\phi A_s}\left(A_s\frac{\partial u_s}{\partial \phi}+A_\phi\frac{\partial u_\phi}{\partial s}-\frac{\partial A_\phi}{\partial s}u_\phi-\frac{\partial A_s}{\partial \phi}u_s\right),$$

$$\kappa_\phi = \frac{1}{A_\phi}\frac{\partial \beta_\phi}{\partial \phi} + \frac{1}{A_\phi A_s}\frac{\partial A_\phi}{\partial s}\beta_s,$$

$$\kappa_s = \frac{1}{A_s}\frac{\partial \beta_s}{\partial s} + \frac{1}{A_\phi A_s}\frac{\partial A_s}{\partial \phi}\beta_\phi,$$

$$\bar{\kappa}_{\phi s} = \frac{1}{2A_\phi A_s}\left\{A_s\frac{\partial \beta_s}{\partial \phi} + A_\phi\frac{\partial \beta_\phi}{\partial s} - \frac{\partial A_\phi}{\partial s}\beta_\phi - \frac{\partial A_s}{\partial \phi}\beta_s + \frac{1}{2}\left(\frac{1}{R_s} - \frac{1}{R_\phi}\right)\left[\frac{\partial}{\partial \phi}(A_s u_s) - \frac{\partial}{\partial s}(A_\phi u_\phi)\right]\right\} \tag{9}$$

3.3. Constitutive law

In the ϕ and s directions, respectively, the moduli of elasticity are denoted by E_ϕ and E_s, and the values of Poisson's ratio are ν_ϕ and ν_s. The in-plane shear modulus is $G_{\phi s}$ and the thickness of the shell is h.

The stress–strain relationships are assumed to be (e.g., Reddy, 1984; Jones, 1999)

$$N_\phi = A_{11}(\varepsilon_\phi + \nu_s\varepsilon_s), \quad N_s = A_{22}(\varepsilon_s + \nu_\phi\varepsilon_\phi), \quad \bar{N}_{\phi s} = A_{66}\gamma_{\phi s}$$

$$M_\phi = D_{11}(\kappa_\phi + \nu_s\kappa_s), \quad M_s = D_{22}(\kappa_s + \nu_\phi\kappa_\phi), \quad \bar{M}_{\phi s} = 2D_{66}\bar{\kappa}_{\phi s} \tag{10}$$

where

$$A_{11} = \frac{E_\phi h}{1-\nu_\phi\nu_s}, \quad A_{22} = \frac{E_s h}{1-\nu_\phi\nu_s}, \quad A_{66} = G_{\phi s}h$$

$$D_{11} = \frac{E_\phi h^3}{12(1-\nu_\phi\nu_s)}, \quad D_{22} = \frac{E_s h^3}{12(1-\nu_\phi\nu_s)}, \quad D_{66} = \frac{G_{\phi s}h^3}{12} \tag{11}$$

For later use, the following quantities are also defined:

$$A_{12} = A_{11}\nu_s = A_{22}\nu_\phi, \qquad D_{12} = D_{11}\nu_s = D_{22}\nu_\phi \tag{12}$$

4. Solution procedure

Approximate solutions will be obtained using the Rayleigh–Ritz method. The elastic strain energy U_E, potential U_{I} of the initial stresses, and potential U_{L} of the service loads are as follows:

$$U_E = \frac{1}{2}\int_{-s_0}^{s_0}\int_0^{2\pi}\left(A_{11}\varepsilon_\phi^2 + 2A_{12}\varepsilon_\phi\varepsilon_s + A_{22}\varepsilon_s^2 + A_{66}\gamma_{\phi s}^2\right)A_\phi A_s\,\mathrm{d}\phi\,\mathrm{d}s$$

$$+\frac{1}{2}\int_{-s_0}^{s_0}\int_0^{2\pi}\left(D_{11}\kappa_\phi^2 + 2D_{12}\kappa_\phi\kappa_s + D_{22}\kappa_s^2 + 4D_{66}\bar{\kappa}_{\phi s}^2\right)A_\phi A_s\,\mathrm{d}\phi\mathrm{d}s \tag{13a}$$

$$U_{\mathrm{I}} = \frac{1}{2}\int_{-s_0}^{s_0}\int_0^{2\pi}\left[T_\phi\beta_\phi^2 + 2T_{\phi s}\beta_\phi\beta_s + T_s\beta_s^2\right]A_\phi A_s\,\mathrm{d}\phi\mathrm{d}s \tag{13b}$$

$$U_{\mathrm{L}} = -\int_{-s_0}^{s_0}\int_0^{2\pi}(q_\phi u_\phi + q_s u_s + q_n w)A_\phi A_s\,\mathrm{d}\phi\mathrm{d}s \tag{13c}$$

The total potential is $U = U_E + U_{\mathrm{I}} + U_{\mathrm{L}}$.

Kinematically admissible functions $f_i(s, \phi)$ are chosen for the displacements, which are written in the form

$$u_\phi(s,\phi) = \sum_{i=1}^{n_1} d_i f_i(s,\phi), \quad u_s(s,\phi) = \sum_{i=n_1+1}^{n_2} d_i f_i(s,\phi), \quad w(s,\phi) = \sum_{i=n_2+1}^{n_3} d_i f_i(s,\phi) \tag{14}$$

These expressions are used in the total potential U, and the first partial derivative of U with respect to each of the coefficients d_i is set equal to zero. The resulting set of linear equations is solved for the coefficients. The software package 'Mathematica' (Wolfram, 1996) is utilized to carry out the numerical computations in the solution procedure.

5. Numerical results

In this section the internal pressure is assumed to be $p = 400$ kPa. Under this pressure, the centerline of the arch is assumed to be semi-circular (i.e., κ is constant), with $s_0 = 20$ m and hence $\kappa = \pi/40$ m^{-1}. The cross-sectional radius is chosen to be $r = 0.15$ m and the thickness to be $h = 2.5$ mm. The material is assumed to be homogeneous and isotropic, with $E_\phi = E_s = 7$ GPa, $\nu_\phi = \nu_s = 0.3$, and $G_{\phi s} = 2.69$ GPa in the pressurized state. At the bases, the arch is assumed to have no vertical displacement u_s, no radial displacement w, and no slope $\partial w/\partial s$. The functions f_i used in Eq. (14) will depend on the symmetry properties of the service load under consideration.

5.1. Full snow load

In this case, a vertical load is applied with uniform intensity q per unit horizontal area, as shown in Fig. 1(a). It is assumed that the snow will fall off the arch if $|\phi| > \pi/6$ or $|\psi| > \pi/6$, where ψ is the angle in the xy plane of the centerline tangent with the horizontal (i.e., $\psi = \theta - (\pi/2)$, where θ is shown in Fig. 1(a)). The load components used in Eq. (13c) are

$$q_\phi = q\cos^2\psi\sin\phi\cos\phi, \quad q_s = q\sin\psi\cos\psi\cos\phi, \quad q_n = -q\cos^2\psi\cos^2\phi \tag{15}$$

It is convenient to write the functions f_i in terms of the nondimensional meridional coordinate $\xi = (s + 20)/40$, where s is in meters, so that $\xi = 0$ when $s = -s_0$ and $\xi = 1$ when $s = s_0$ (see Fig. 1(a)). For this case with symmetry in the load with respect to two vertical planes, the functions $\sin(n\phi)\cos(2m\pi\xi)$, $n = 1, 2$, $m = 0, 1, \ldots, 4$ are used for u_ϕ; $\cos(n\phi)\sin(2m\pi\xi)$, $n = 0, 1, 2$, $m = 1, \ldots, 4$ are used for u_s; and $\cos(n\phi)[1 - \cos(2m\pi\xi)]$, $n = 0, 1, 2$, $m = 1, \ldots, 4$ are used for w. In this example and all the following ones, the terms involving 2ϕ turn out to have negligible coefficients, and therefore they will not be mentioned further. Thus the circular cross sections remain essentially circular for the distributed loads treated here.

The dominant terms in the solution are listed in Appendix A, and the nondimensional displacements $\tilde{u}_s$ and $\tilde{w}$ along the top meridian are plotted versus ξ in Fig. 3, where

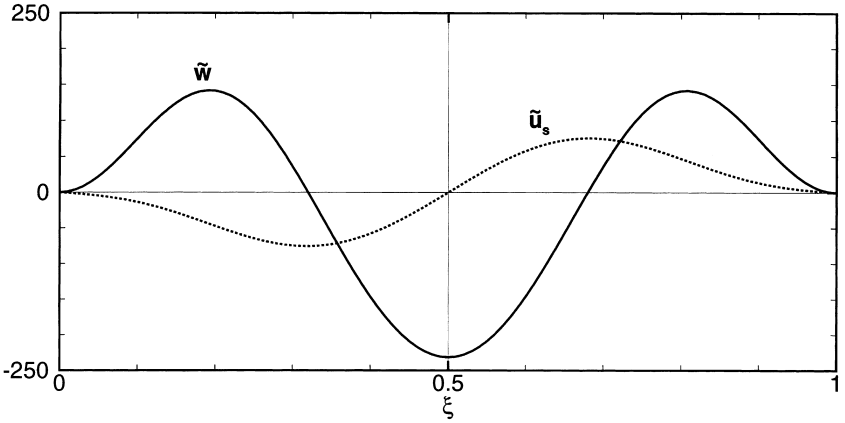

Fig. 3. Deflections along top meridian for full snow load.

$$\tilde{u}_s = \frac{u_s p}{rq}, \qquad \tilde{w} = \frac{wp}{rq} \tag{16}$$

Naturally, u_s is anti-symmetric and w is symmetric about the crown, whereas $u_\phi = 0$ on the top meridian. A side view of the resulting displaced arch is illustrated in Fig. 4, using a large value of the load so that the shape is distinguished from the light (semi-circular) shape of the initial state. The central region of the arch deflects downward and the outer regions bulge outward.

5.2. Half snow load

Now the loading is assumed to consist of the right half of the uniform load shown in Fig. 1(a). Hence, it is symmetric with respect to ϕ but not with respect to s. The chosen functions are $\sin(\phi)\cos(m\pi\xi)$, $m = 0, 1, \ldots, 8$ for u_ϕ; $\cos(n\phi)\sin(m\pi\xi)$, $n = 0, 1$, $m = 1, \ldots, 8$ for u_s; and $\cos(\phi)[1 - \cos(m\pi\xi)]$, $m = 1, \ldots, 8$ for w.

Some of the functions for w do not satisfy the boundary condition $w = 0$ at $\xi = 1$, the right base. For this case, distributed radial springs are added at $\xi = 1$ with high stiffness coefficient $C = 10^6 p$ so that this condition will be satisfied approximately.

Therefore, the potential U_B of the springs is given by

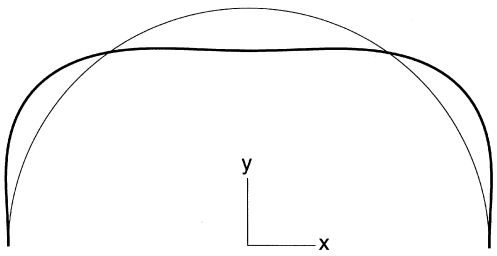

Fig. 4. Shape of top meridian under full snow load.

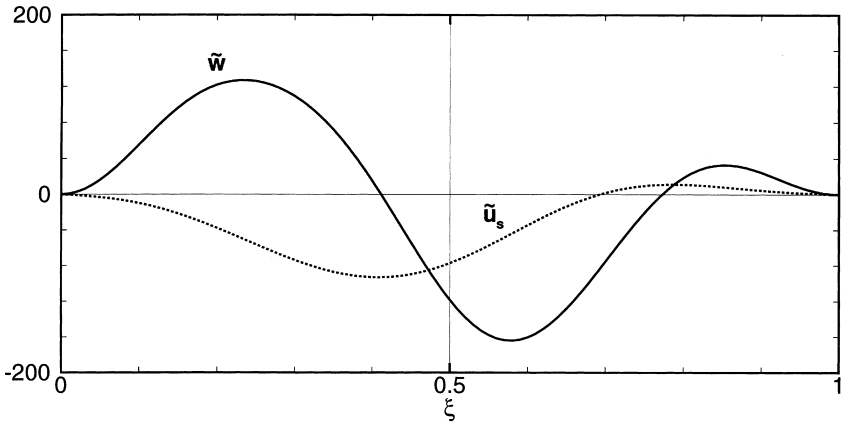

Fig. 5. Deflections along top meridian for half snow load.

$$U_B = \frac{1}{2}C\int_0^{2\pi} w^2(s_0, \phi)\, \mathrm{d}\phi \tag{17}$$

is included in the total potential U before the stationarity conditions are obtained.

The dominant terms are given in Appendix A, the variations of u_s and w along the top meridian are shown in Fig. 5, and the side view is depicted in Fig. 6. With the downward load applied on the right of the center, the arch has a greater outward bulge on the left side than on the right side.

5.3. Wind load

The wind is assumed to flow from left to right in Fig. 1(a). The angle θ is shown in the figure. The normal pressure distribution from the wind is taken to be

$$q_n = -0.5\rho v^2 q k(\theta)\cos\phi, \quad -\pi/4 < \phi < \pi/4 \tag{18}$$

where ρ is the density of air, v is the speed of the wind, and $k(\theta)$ is chosen to be the 'rough' distribution from Soare (1967), which is given by the formula

$$k(\theta) = -0.258 + 0.488\cos\theta + 0.476\cos 2\theta + 0.328\cos 3\theta + 0.100\cos 4\theta \tag{19}$$

and is plotted in Fig. 7.

As in the previous section, the loading is symmetric with respect to ϕ but not with respect to s, and

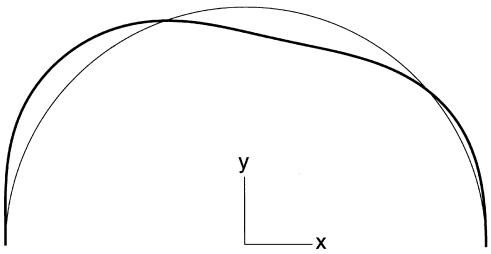

Fig. 6. Shape of top meridian under half snow load.

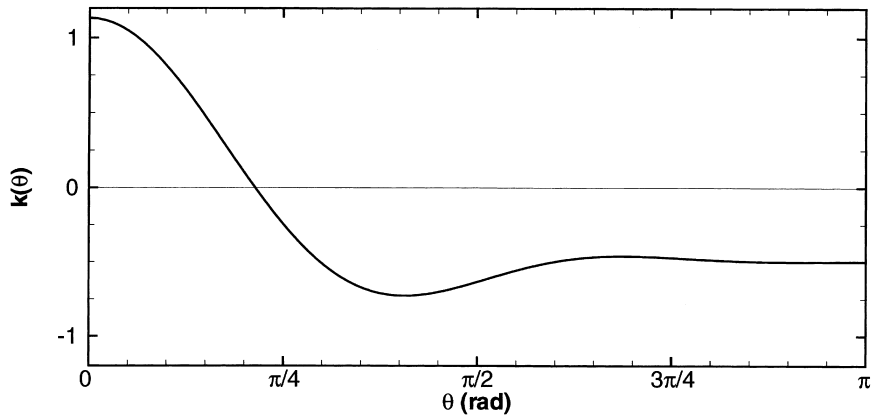

Fig. 7. Distribution of wind load along arch.

the same functions f_i are used here. The results are listed in Appendix A and are plotted in Figs. 8 and 9 for the top meridian. External pressure near the left base causes an inward deflection for most of the left half of the arch in Fig. 9.

5.4. Side load

In this last example, the load is symmetric in s but not in ϕ. It is given by $q_n = -q$ for $-s_0/2 < s < s_0/2$ and $\pi/4 < \phi < 3\pi/4$. That is, the load acts normally in Fig. 1(a) over the top half of the arch along the s direction and over the middle of the cross section on the front side.

The functions $\cos(n\phi)\cos(2m\pi\xi)$ and $\sin(n\phi)\cos(2m\pi\xi)$, $n = 0, 1$, $m = 0, 1, 2, 3$ are used for u_ϕ; $\cos(n\phi)\sin(2m\pi\xi)$ and $\sin(n\phi)\sin(2m\pi\xi)$, $n = 0, 1$, $m = 1, 2, 3$ are used for u_s; and $\cos(n\phi)[1 - \cos(2m\pi\xi)]$ and $\sin(n\phi)[1 - \cos(2m\pi\xi)]$, $n = 0, 1$, $m = 1, 2, 3$ are used for w. Numerical results are given in Appendix A, and the horizontal displacement at the center of the front side of the arch (i.e., at $\phi = \pi/2$) is plotted versus ξ in Fig. 10.

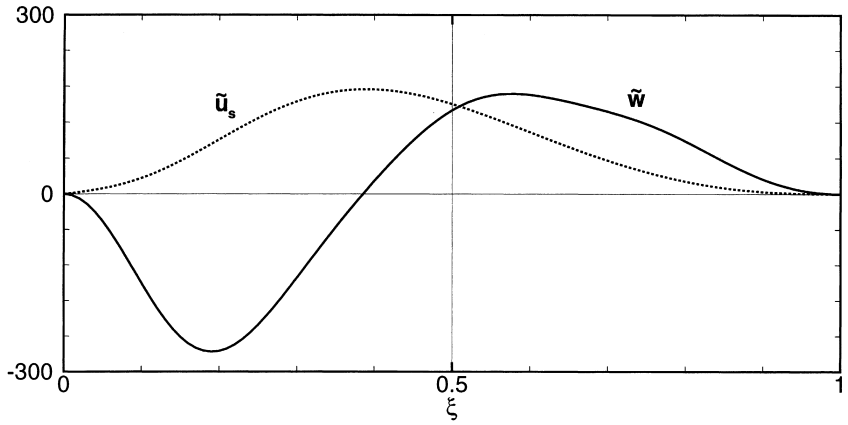

Fig. 8. Deflections along top meridian for wind load.

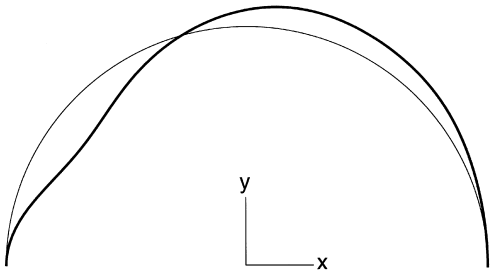

Fig. 9. Shape of top meridian under wind load.

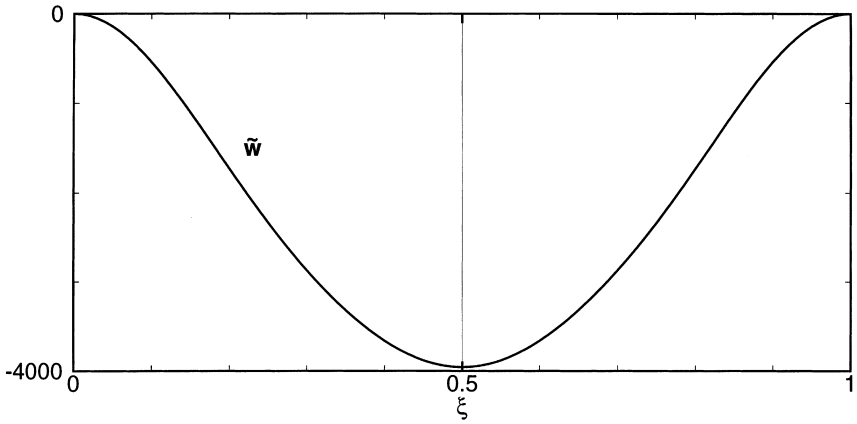

Fig. 10. Deflection along top meridian for side load.

6. Concluding remarks

Inflatable arches made of a flexible fabric-like material have been considered. The starting point for the analysis was the configuration of the arch after it was pressurized, and the geometry was based on this pressurized state. The cross section was assumed to be circular with a constant radius, but the profile of the centerline of the cross sections was arbitrary. It was assumed that only membrane stresses are significant in this initial state. A closed-form solution for these stresses was given, which reduces to a standard solution for the case of a toroidal shell with a circular profile.

Distributed loads were then applied to the arch. The linear thin-shell theory of Sanders, including membrane and bending stresses, was utilized to formulate the governing equations. Naturally, the initial stresses appear in the equilibrium equations. The material was assumed to be linearly elastic and was allowed to be nonhomogeneous and orthotropic. The Rayleigh–Ritz method was applied to obtain approximate expressions for the displacements, which then can be used to determine strains and stress resultants.

In the numerical examples, the profile was assumed to be semi-circular, the bases were fixed in the vertical and radial directions, and the material was homogeneous and isotropic. The choice of assumed displacement functions depended on the symmetry properties of the load. For the full snow load there

was symmetry with respect to both meridional and circumferential coordinates s and ϕ, for the half snow load and wind load there was symmetry only in ϕ, and for the side load there was symmetry only in s.

If the terms involving bending and twisting moments are deleted from the total potential, the results are only altered slightly. Therefore, the distributed loads considered here do not lead to significant moments. However, if other loading conditions were treated, such as a concentrated load at the crown, the moments would become important.

There is increased interest in the use of fabrics in architecture (e.g., Kronenburg, 1995, 1996; Berger, 1996; Schock, 1997). Membrane structures for use on the moon or Mars also have received some study (Chow, 1992; Sadeh and Criswell, 1995; Kronenburg, 1996). Applications of inflatable arches such as considered here may increase substantially in the future.

Acknowledgements

This research was supported by the U.S. Army Research Office under Grant No. DAAH04-95-1-0175 (Dr. Gary L. Anderson, monitor). The authors gratefully acknowledge helpful discussions with Prof. Rakesh K. Kapania (Department of Aerospace and Ocean Engineering).

Appendix A

For the examples in Section 5, the dominant terms in the displacements are given here. In the case of the full snow load,

$$\tilde{u}_s = (-65.54 + 2.31\cos\phi)\sin 2\pi\xi + (28.23 - 4.95\cos\phi)\sin 4\pi\xi$$
$$+(2.52 - 1.03\cos\phi)\sin 6\pi\xi - 0.10\cos\phi\sin 8\pi\xi \tag{A1}$$

$$\tilde{w} = (-2.12 + 130.86\cos 2\pi\xi - 112.59\cos 4\pi\xi$$
$$-15.09\cos 6\pi\xi - 1.06\cos 8\pi\xi)\cos\phi \tag{A2}$$

$$\tilde{u}_\phi = -\tilde{w}\tan\phi \tag{A3}$$

For the example with the half snow load, they are given by

$$\tilde{u}_s = -54.79\sin\pi\xi + (-33.45 + 1.18\cos\phi)\sin 2\pi\xi$$
$$+(22.07 - 2.07\cos\phi)\sin 3\pi\xi + (14.02 - 2.46\cos\phi)\sin 4\pi\xi$$
$$+(-2.89 + 0.81\cos\phi)\sin 5\pi\xi + (1.25 - 0.51\cos\phi)\sin 6\pi\xi$$
$$+(0.48 - 0.26\cos\phi)\sin 7\pi\xi + (0.30 - 0.21\cos\phi)\sin 8\pi\xi \tag{A4}$$

$$\tilde{w} = (-0.98 + 55.07\cos\pi\xi + 66.77\cos 2\pi\xi - 66.20\cos 3\pi\xi$$

$$-55.97\cos 4\pi\xi + 14.44\cos 5\pi\xi - 7.50\cos 6\pi\xi$$

$$-3.31\cos 7\pi\xi - 2.32\cos 8\pi\xi)\cos\phi \tag{A5}$$

and Eq. (A3). For the example with the wind load,

$$\tilde{u}_s = 132.17\sin\pi\xi + (44.74 - 1.58\cos\phi)\sin 2\pi\xi$$

$$+(-25.90 + 2.43\cos\phi)\sin 3\pi\xi + (-15.26 + 2.68\cos\phi)\sin 4\pi\xi$$

$$+(-8.40 + 2.35\cos\phi)\sin 5\pi\xi + (-3.24 + 1.32\cos\phi)\sin 6\pi\xi$$

$$+(-1.80 + 1.00\cos\phi)\sin 7\pi\xi + (-0.85 + 0.62\cos\phi)\sin 8\pi\xi \tag{A6}$$

$$\tilde{w} = (2.21 - 132.17\cos\pi\xi - 89.43\cos 2\pi\xi + 77.64\cos 3\pi\xi$$

$$+61.00\cos 4\pi\xi + 41.94\cos 5\pi\xi + 19.43\cos 6\pi\xi$$

$$+12.58\cos 7\pi\xi + 6.80\cos 8\pi\xi)\cos\phi \tag{A7}$$

and Eq. (A3) is satisfied. Finally, for the example with the side load,

$$\tilde{u}_s = (-0.19 + 45.69\sin\phi)\sin 2\pi\xi + (0.07 + 8.31\sin\phi)\sin 4\pi\xi$$

$$+2.59\sin\phi\sin 6\pi\xi \tag{A8}$$

$$\tilde{w} = (-2{,}155.9 + 1{,}941.7\cos 2\pi\xi + 177.2\cos 4\pi\xi$$

$$+37.0\cos 6\pi\xi)\sin\phi \tag{A9}$$

$$\tilde{u}_\phi = \tilde{w}\cot\phi \tag{A10}$$

References

Berger, H., 1996. Light Structures, Structures of Light. Birkhäuser, Basel.

Budiansky, B., Radkowski, P.P., 1963. Numerical analysis of unsymmetrical bending of shells of revolution. AIAA Journal 1, 1833–1842.

Budiansky, B., Sanders, J.L. Jr, 1963. On the 'best' first-order linear shell theory. In: Progress in Applied Mechanics. Macmillan, New York, pp. 129–140.

Carradine, D.M., Plaut, R.H., 1998. Experiments on the response of arch-supported membrane shelters to snow and wind loading. International Journal of Space Structures 13, 197–202.

Chow, P.Y., 1992. Construction of pressurized self-supporting membrane structure. Journal of Aerospace Engineering 5, 274–281.

Dent, R.N., 1972. Principles of Pneumatic Architecture. Wiley, New York.

Galas, B., Bacskai, A., 1998. International achievement awards. Fabrics and Architecture 10 (2), 19–41.

Hampel, J.W., Brown, G.J., Sharpless, G.C., 1996. High pressure inflatable structures incorporating highly oriented fibers. In: Proceedings of the 20th Army Science Conference: Science and Technology for Force XXI, vol. 2, 953–957.

Jones, R.M., 1999. Mechanics of Composite Materials, 2nd ed. Taylor and Francis, Philadelphia.
Kawaguchi, M., Chin, Y., Hosogaya, T., Tanaka, A., Oki, H., Baba, T., Mochizuki, T. 1972. Engineering problems of pneumatic structures. In: Yokoo, Y., Nakamura, T., Heki, K., Kawamata, S. (Eds.), Tension Structures and Space Frames. Architectural Institute of Japan, Tokyo, pp. 449–460.
Kim, J.-Y., Plaut, R.H., Kwun, T.-J., 1998. Analysis of tent-like structures supported by pressurized fabric arches. In: Hough, R., Melchers, R. (Eds.), Lightweight Structures in Architecture, Engineering and Construction, vol. 2. Lightweight Structures Association of Australia, Randwick, New South Wales, pp. 821–829.
Koiter, W.T., 1960. A consistent first approximation in the general theory of thin elastic shells. In: Proceedings of the IUTAM Symposium on the Theory of Thin Elastic Shells, North-Holland, Amsterdam, 12–33.
Kraus, H., 1967. Thin Elastic Shells. Wiley, New York.
Kronenburg, R., 1995. Tensile architecture. Architectural Design: A.D. 65 (9/10), 8–15.
Kronenburg, R., 1996. Portable Architecture. Architectural Press, Oxford.
Lukasiewicz, S., Balas, L., 1990. Collapse loads of a cylindrical or toroidal free-standing inflatable membrane. Mechanics of Structures and Machines 18, 499–513.
Mohan, P., Kapania, R.K., 1998a. Updated Lagrangian formulation of a flat triangular element for thin laminated shells. AIAA Journal 36, 273–281.
Mohan, P., Kapania, R.K., 1998b. Analysis of general shells under deformation dependent pressure loads using a flat triangular shell element. In: Proceedings of the 39th AIAA/ASME/ASCE/AHS/ASC Structures, Structural Dynamics and Materials Conference, vol. 1, 534–541.
Molloy, S.J., 1998. Finite element analysis of a pair of leaning pressurized arch-shells under snow and wind loads. M.S. thesis, Virginia Polytechnic Institute and State University, Blacksburg, VA.
Molloy, S.J., Plaut, R.H., Kim, J.-Y., 1999. Behavior of pair of leaning arch-shells under snow and wind loads. Journal of Engineering Mechanics 125, 663–667.
Otto, F. (Ed.), 1973. Tensile Structures. The MIT Press, Cambridge, MA.
Price, C., Newby, F., Suan, R.H., 1971. Air Structures. Her Majesty's Stationery Office, London.
Reddy, J.N., 1984. Energy and Variational Methods in Applied Mechanics. Wiley, New York.
Reffell, B., 1967. High pressure structures. In: Proceedings of the First International Colloquium on Pneumatic Structures, International Association for Shell Structures, Madrid, 64–67.
Sadeh, W.Z., Criswell, M.E., 1995. Inflatable structures for a lunar base. Journal of the British Interplanetary Society 48, 33–38.
Sanders, J.L., Jr., 1959. An improved first-approximation theory for thin shells. Technical Report TR-R24, NASA, Washington, DC.
Schock, H.-J., 1997. Soft Shells. Birkhäuser, Basel.
Soare, M., 1967. Application of Finite Difference Equations to Shell Analysis. Pergamon, New York.
Steeves, E.C., 1978. Structural behavior of pressure stabilized arches. Technical Report Natick/TR-78/018, U.S. Army Natick Research and Development Laboratories, Natick, MA.
Wolfram, S., 1996. The Mathematica Book, 3rd ed. Wolfram Media, Champaign, IL.
Zhang, F., Redekop, D., 1992. Surface loading of a thin-walled toroidal shell. Computers and Structures 43, 1019–1028.
Zingoni, A., 1997. Shell Structures in Civil and Mechanical Engineering. Thomas Telford, London.